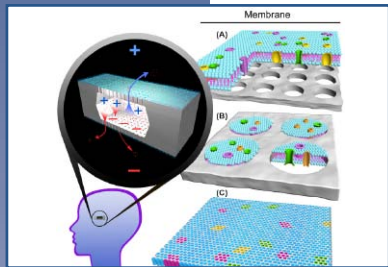
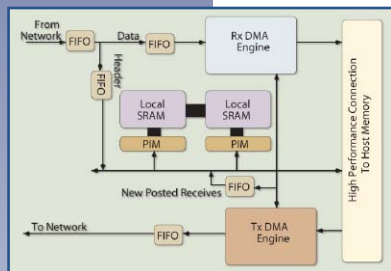




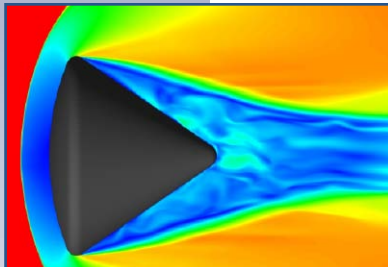
SANDIA NATIONAL LABORATORIES
Science, Technology and Engineering



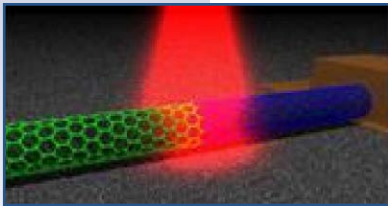
Bioscience



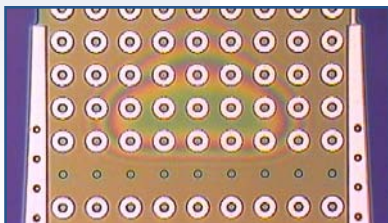
Computers and Information Sciences



Engineering Sciences



Materials Science and Technology



Microelectronics and Microsystems



Pulsed Power

Vision

Sandia National Laboratories is the provider of innovative, science-based, systems-engineering solutions to our Nation's most challenging national security problems.

Mission

Committed to "science with the mission in mind," Sandia creates innovative, science-based, systems-engineering solutions that

- sustain, modernize, and protect our nuclear arsenal,
- prevent the spread of weapons of mass destruction,
- provide new capabilities for national defense,
- defend against terrorism,
- protect our national infrastructures, and
- ensure stable sources of energy and other critical resources.

Guiding principles for ST&E

- Ensure that the fundamental science and engineering core is vibrant and pushing the forefront of knowledge
- Enable the programs by effective application of that science base
 - ♦ responding to current needs
 - ♦ anticipating the future

About Science Matters!

The purpose of *Science Matters!* is to publicize and celebrate recent Sandia accomplishments in science, technology, and engineering. We feature the science that underpins and enables technology for Sandia's missions. We nurture expertise, facilities and equipment to create world-class science that pushes the frontiers of knowledge and anticipates future mission needs. New *Science Matters!* are being issued semiannually.

Vice President & Chief Technology Officer
Rick Stulen, Ph.D.
505-844-5148
rhstule@sandia.gov

Deputy, Science & Technology
Wendy Cieslak, Ph.D.
844-8633
wrciesl@sandia.gov

Science Matters! Point of Contact
Alan Burns, Ph.D.
505-844-9642
aburns@sandia.gov





Materials Sciences & Technology Biomaterials



Figure 1: (Left) An intact bovine cornea being pressurized. The cornea appears green-blue due to illumination coming from inside the pressure chamber. Speckles on the surface of the cornea are graphite particles used to create contrast for 3D digital image correlation. At the edge of the cornea, the intact tissue is held rigidly using a custom saddle-shaped fixture that was designed and fabricated directly from a 3D image of the ocular globe.

Cornea Mechanics: Probing Bio-engineered Materials

Explaining the mechanical behavior of corneas leads to new general theory of viscous-fiber reinforced composite materials.

Technical Contact:

Brad Boyce
505-845-7525
blboyce@sandia.gov

Reese Jones
925-294-4744
rjones@sandia.gov

Science Matters Contact:

Alan Burns, Ph.D.
505-844-9642
aburns@sandia.gov

The eye is a magnificently engineered opto-electro-mechanical device. Clinicians and researchers are continuously striving to better understand the connections between the eye's anatomy and its functionality. In the case of the cornea, the transparent curved membrane at the front of the eye that refractively gathers and helps to focus light, the fixed shape is critical. Thus mechanical response of the cornea is relevant to diseases (e.g., keratoconus), surgical procedures (e.g., LASIK), prosthetics, and clinical practice. In glaucoma screening, a "tonometer" probe is used to deform the patient's cornea, thereby indirectly measuring intraocular pressure based on an assumed stiffness of the cornea. To better understand the mechanical response of cornea tissue and its relation to the underpinning structure of the cornea, Sandia is applying decades of experience in mechanical behavior of materials.

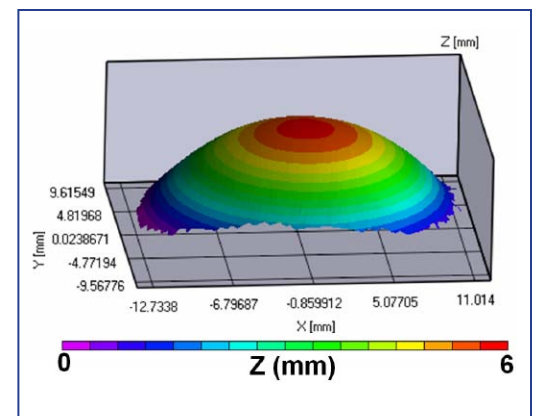


Figure 2: A 3D map of the shape of the cornea. These maps are acquired in real-time to track the pressure-driven deformation of the cornea during inflation testing.

To study the properties of this complex tissue, researchers originally used a conventional tensile test on a strip of bovine cornea. However, the tensile test fails to mimic the biaxial loading condition of real eyes. To remedy this problem, Sandia researchers developed a whole-cornea inflation test that mimics real physiologic deformation. As the entire cornea is inflated while still attached to the white sclera of the ocular globe (Figure 1), the deformation is mapped with real-time, high-resolution 3D digital image correlation (Figure 2).

These tests revealed an intricate time-dependent deformation response that could not be described with existing theory. Instead, Sandia developed a new theory based on the orientation and distribution

of collagen fibrils, the primary structural component of the cornea. This theory, which matches experiments extraordinarily well (Figure 3), has since been generalized to describe a wide range of viscous-fiber reinforced composite materials.

One of the most interesting insights provided by Sandia's research is that the material near the center of the cornea deforms very little during pressure fluctuations: most of the necessary deformation is accommodated around the periphery. This is due to the density and orientation of collagen fibrils in the central cornea, compared to the lower density of circumferentially-oriented fibrils in the periphery. The result of this brilliantly bio-engineered tissue is that our primary vision through the central cornea is largely unaffected by pressure changes.

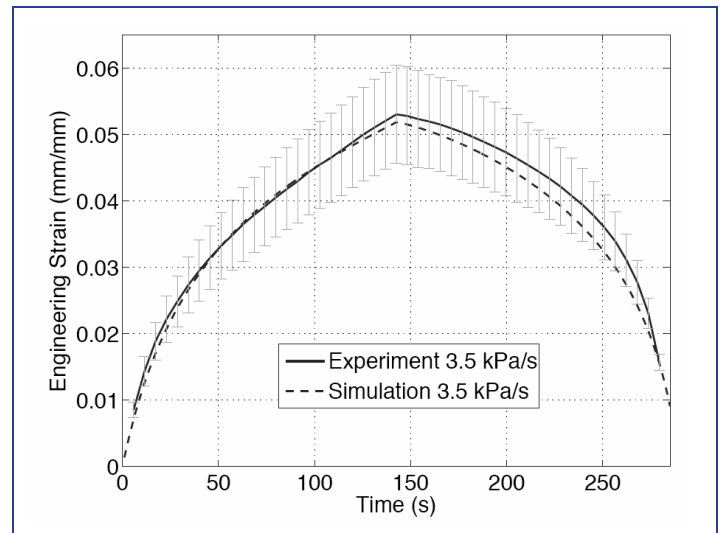


Figure 3: Agreement between experimental results (shown in dashed lines with error bars representing the standard deviation of 9 tests) and predictions using the newly developed multi-mode viscous-fiber composite theory.



Pulsed Power Extreme environments

Pushing Water to the Limit: Ultrafast Solidification in the Sandia Z Machine

Pulsed magnetic compression can be used to examine extremely rapid phase transitions.

The formation of ice by cooling water is slow because ice crystals must first be nucleated on a "seed." However, by using compression at extremely high pressures rather than cooling, seeding is not required and solidification conditions can be rapidly created in water. This allows us to study the fundamental time scales of the phase transition.

Water can exist in many different solid forms at extreme pressure. Above 2 GPa (approximately twenty thousand atmospheres), water becomes ice VII, a dense solid stable beyond 300 K. To reach these states, researchers at Sandia utilize isentropic compression techniques to bring water to extreme pressures while maintaining moderate temperature. As shown in Figure 1, isentropic compression of liquid water enters the ice VII region near 3 GPa. Interestingly, solidification still does not instantly occur at this pressure unless a nucleating seed is present.

Using pulsed magnetic compression in the Sandia Z machine, small water samples (about 3 mg) at atmospheric pressure are squeezed up to 10 GPa in approximately 200 ns. Rapid solidification does occur under these conditions, and is studied by tracking the water sample interface with an optical interferometer. A smooth, continuous motion of the interface during compression indicates a liquid phase; when the transformation to solid water occurs, there is an abrupt, discontinuous motion. Ultra-pure water shows liquid-like behavior until the pressure reaches approximately 7 GPa. At higher pressures, water contracts in just a few nanoseconds and solidifies as indicated by the discontinuous motion in the interferometer. Experiments with different container materials yielded identical results, suggesting that

solidification occurs throughout the compressed water sample, not simply at the water-container boundary.

This work reveals that 7 GPa is the experimental limit to isentropic compression of liquid water, information critical in the study of dynamic material behavior. It is also significant that the time scales probed in this work approach the domain of molecular dynamics, thus providing a potential benchmark for numerical simulations of solidification.

For more information:

Technical Contact:

Daniel Dolan
505-284-8608
dhdolan@sandia.gov

Science Matters Contact:

Alan Burns, Ph.D
505-844-9642
aburns@sandia.gov

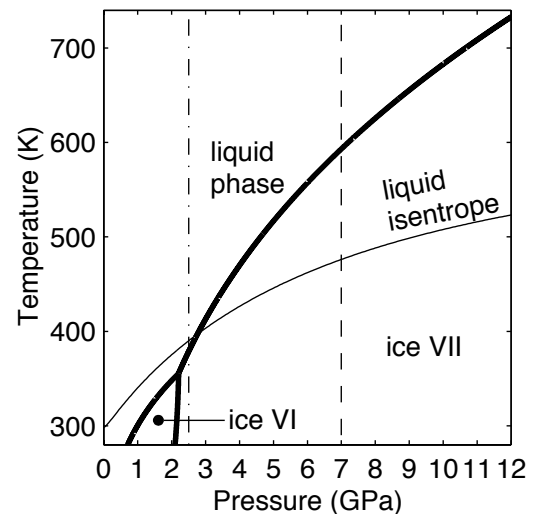
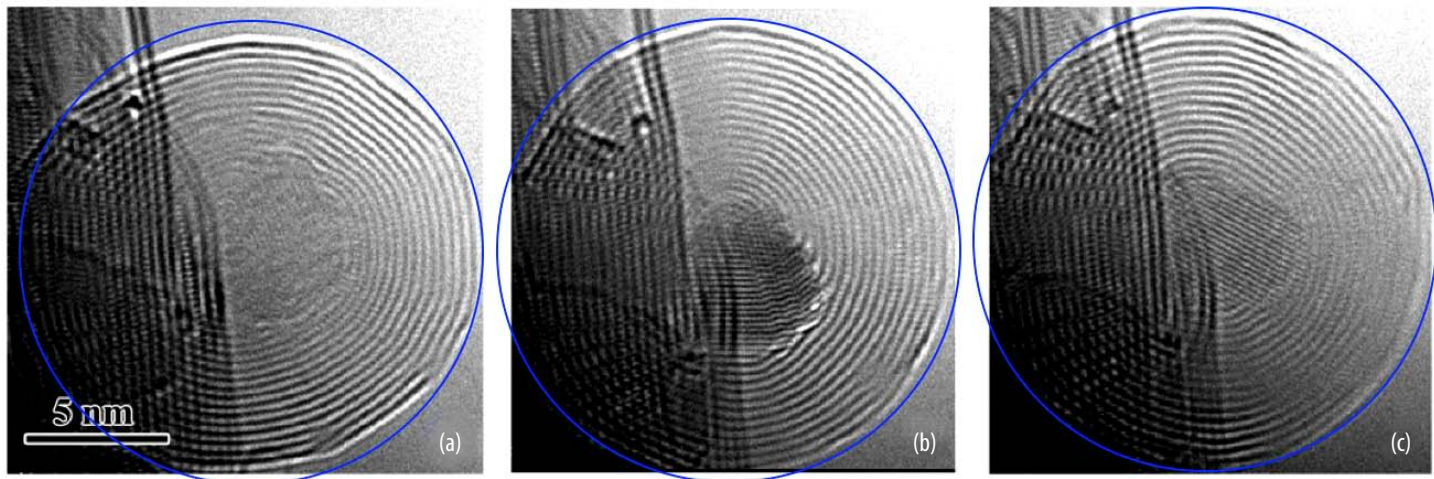


Figure 1: Heavy lines indicate the boundaries between different forms of water. The solid line shows the temperature-pressure path of liquid water under isentropic compression, which crosses the ice VII boundary near 3 GPa (left dashed line). Ultrafast solidification is observed at 7 GPa (right dashed line).



Materials Science and Technology Nanoscience



In-situ Observation of “Molten” Diamond

Nanoscale carbon structures allow researchers to simultaneously achieve the extremely high pressures and temperatures needed to melt diamond.

For more information:

Technical Contact:

Jiayu Huang
505-284-5963
jhuang@sandia.gov

Science Matters Contact:

Alan Burns, Ph.D
505-844-9642
aburns@sandia.gov

The behavior of materials under extreme conditions of high pressure and temperature has long been of interest to researchers in physics, astronomy, and geology. Since diamond possesses the highest hardness, thermal conductivity, and melting temperature of all materials, it has been the focus of numerous studies at extreme conditions. Under normal atmospheric pressure and very high temperatures, diamond does not melt but instead turns into graphite. It is believed that melting will occur only at both extremely high pressures and temperatures. Until now, no one had been able to simultaneously achieve these conditions *in-situ* for melting diamond.

Sandia researchers created these extreme conditions for melting at the nanoscale. They used carbon nanotubes as high-temperature heaters and spherical “carbon onions” as high pressure cells (Fig. 1). The onions are roughly spherical nanoscale concentric shells of graphite-like carbon that are bound to the nanotubes. By heating the onions via the nanotubes, and then applying electron beam irradiation, the temperatures inside the onions can be raised to higher than 2000°C. Furthermore,

because the outer onion layers act essentially as a containment cell, pressures of up to 400,000 atmospheres are obtained in the center. Observations through a transmission electron microscope (TEM) showed that under these conditions, the diamond was formed and underwent a kind of “quasi-melting,” in which the diamond fluctuates between crystal forms by continually melting and refreezing in a different configuration (size, shape, internal structure, and crystal orientation, Fig. 1).

This is the closest anyone has ever come to directly melting diamond. No one really knows what molten carbon looks like. The graphite form seems to break down into liquid-like blobs when heated to high temperatures, although they have not been examined while still molten. Our discovery offers unprecedented opportunities to studying the structures of carbon at extreme conditions *in-situ* and at an atomic-scale. On the geologic scale, these studies may increase our understanding of the extreme conditions in the earth’s mantle.

Figure 1: (Above) Sequential transmission electron microscopy (TEM) images showing quasi-melting of diamond crystals at the center of a “carbon onion.” The diamond crystal structure at the center fluctuates from a polycrystal (a) to a multiple twinned crystal (b), to a single crystal (c) in a matter of seconds.



Sandia
National
Laboratories





PUBLICATIONS

The results were published this summer in *Nano letters* [1], and a news article about the results appeared in the July 26, 2007, issue of *Nature* [2].

References

1. J.Y. Huang, *Nano letters* 7, 2335 (2007).
2. P. Ball, *Nature* 448, 396 (2007).



Engineering Sciences Fluid Science

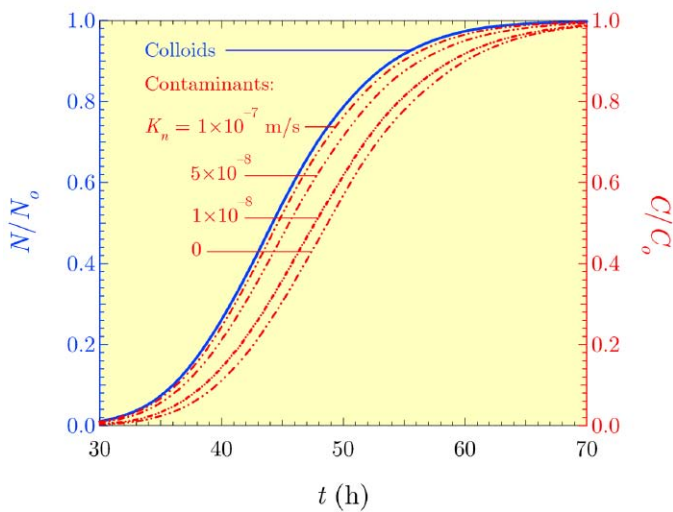


Figure 1: Normalized colloid (blue) and contaminant (red) breakthrough curves where increasing reaction rate of the contaminants with the colloids collapses the contaminant curve onto the colloid curve. Here, no natural attenuation processes are considered.

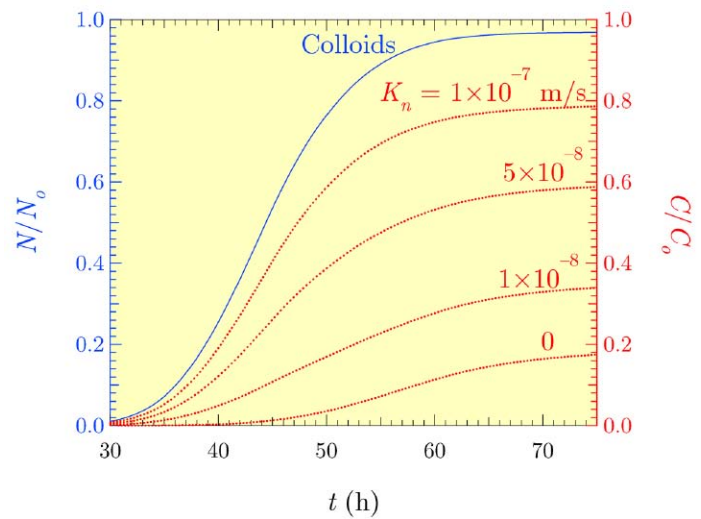


Figure 2: Normalized colloid and contaminant curves when natural attenuation processes retard breakthrough. Note that still, about 97% of the colloids exit the system, but much fewer contaminants do unless they are associated with the colloids (higher co-transport reaction rates).

Colloids and Buried Radioactive Waste

Sorption of contaminants onto colloids can dramatically affect their mobility in porous media.

For more information:

Technical Contact:
Scott James
925-294-2616
scjames@sandia.gov

Science Matters Contact:
Alan Burns, Ph.D
505-844-9642
aburns@sandia.gov

Hazardous wastes, especially radioactive materials, are often disposed in canisters and buried in deep, fractured, low-permeability rock formations (e.g., granite, mudstone, shale, volcanic rock, and clay). The science behind safe, deep geologic sequestration and disposal is an enormous concern. For example, the Department of Energy (DOE) has invested considerable effort at the Geologic Repository for the Disposal of Spent Nuclear Fuel and High-Level Radioactive Waste at Yucca Mountain Repository.

In the event of container rupture, dispersal of hazardous waste in groundwater may be aided by colloids, which are very fine particles that range in diameter from the nanometer to the micron scales, and are chemically similar to subsurface material (clay minerals, metal oxides, silicic acid, and organic matter). Colloids are the groundwater equivalent of dust particles in air. Because a colloid has a high surface area per unit mass, it possesses a high sorptive capacity for dissolved contaminants. Thus, contaminants could migrate not only as

dissolved species in the liquid phase, but also when adsorbed onto suspended colloidal particles.

A critical issue, therefore, is whether colloids actually enhance contaminant migration from buried hazardous wastes. To examine this possibility, Sandia researchers are developing colloid-facilitated contaminant transport models. In a model shown here (Figures 1 and 2), colloids and contaminants are introduced at the inlet of a single, variable-aperture fracture. Results represent the ensemble average of 100 stochastic realizations of the geologic fracture and indicate the mass fraction (breakthrough) exiting the fracture outlet. In Figure 1, colloid (blue) and contaminant (red) breakthrough curves are given in the case when there is no natural attenuation for the migration of the dissolved component, such as diffusion into the surrounding matrix or chemical reactions with the fracture surface. In this case, the red curves collapse onto the faster moving colloid curve with increasing reaction tendency (K_n) to bind to the colloids.



The colloids are faster moving because they are excluded from most small pore spaces and tend to stay in the fastest moving portions of the flow field because of shear gradients and resulting pressure differences across their diameters. When natural contaminant attenuation mechanisms are taken into account, the results are dramatically different (Figure 2). In this more realistic case, the colloids essentially shield the contaminants from retardation because they typically do not react with fracture surfaces and cannot penetrate the small pore spaces of the surrounding rock. The models thus show that colloids can serve as efficient carriers for contaminants, and significantly enhance their net migration rate, especially in fractured rock formations.

The models are consistent with observations in the field. For example, at the Nevada Test Site, radionuclide analyses for detonation-cavity samples indicated that substantial fractions of selected nuclides are found on natural colloids. In another example, at two separate sites in Los Alamos, plutonium and americium were detected at orders of magnitude greater distances from the source than predicted by dissolved-contaminant transport models. Clearly, taking into account the potential for colloids to facilitate contaminant transport is a key concern for both national and international repository programs.

Microelectronics and Microsystems Photonics

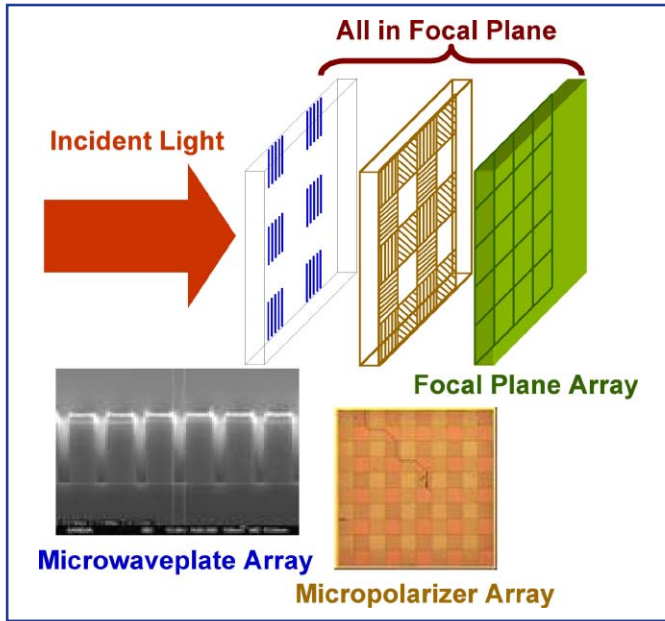


Figure 1: Arrayed components for snapshot polarimetry.

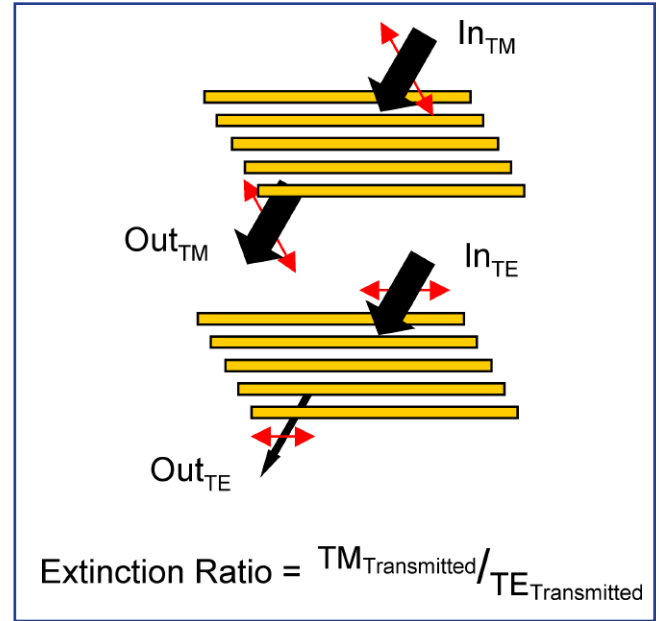


Figure 2: Subwavelength, metallic grid structure for micropolarizers and corresponding extinction ratio. TM, TE are transverse magnetic and electrical vectors of the light wave.

Simultaneous polarization information is used to classify materials and identify objects in remote sensing and military applications.

Snapshot Polarimetric Imaging in the Infrared

Polarimetric imaging measures the polarization states of light coming from all points in a scene. This information, particularly in the infrared region, can help classify materials and identify objects of interest for remote sensing and military applications. Thus there is interest in capturing and storing infrared polarization images in a similar way that intensity information is gathered, i.e., by using a pixelated focal plane array (FPA). Multiple images of a static scene are taken with a combination of oriented polarizers and waveplates in the optical path. Differences between image pairs quantify the distribution, for example, of right circularly polarized light in the scene. Traditionally, sequential polarimetric imaging sensors produce scenes with polarization information through a series of assembled images. However, sequential image capture

is a problem if there is movement from one frame to the next.

Researchers at Sandia have developed a new way, "snapshot polarimetric imaging," (Figure 1) to collect the spatial distribution of all parameters simultaneously. Background noise is also eliminated. To do this, the microsystems engineering facility is used to fabricate features on the subwavelength scale that can directly manipulate the optical fields for each pixel in the FPA. The principle behind linear micropolarizers for long wavelengths is based upon the strong anisotropic absorption of light in a subwavelength, metallic grid structure (Figure 2). The grid structures are patterned with different orientations, defining the polarization axes. The extinction ratio, defined in Figure 2, quantifies micropolarizer performance.

Technical Contact:

Shanalyn Kemme, Ph.D.
505-284-4639
sakemme@sandia.gov

Science Matters Contact:

Alan Burns, Ph.D.
505-844-9642
aburns@sandia.gov

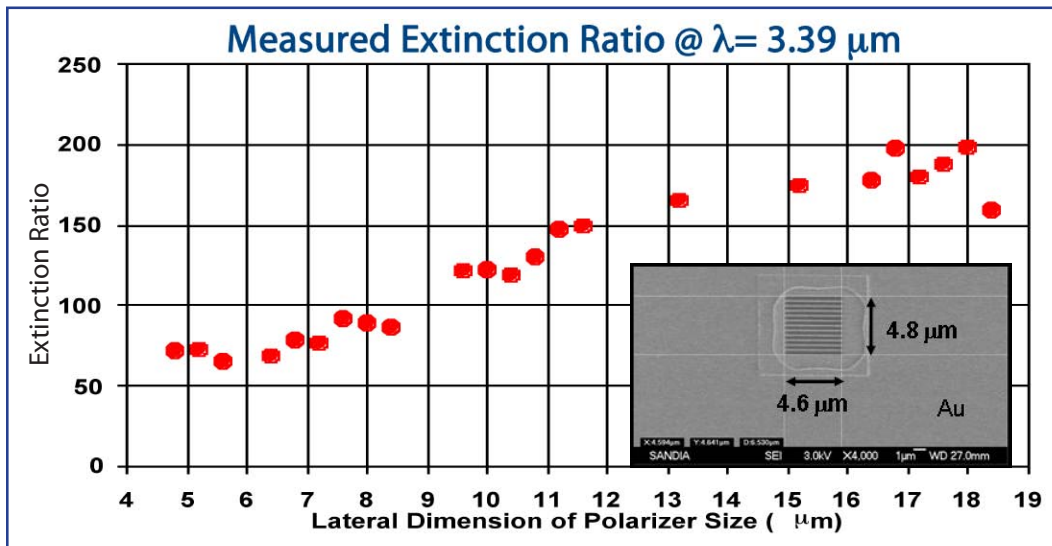


Figure 3: Measured extinction ratio of single, finite aperture micropolarizers at 3.39 microns wavelength. Inset: Scanning electron micrograph of a 4.8 micron pixel polarizer.

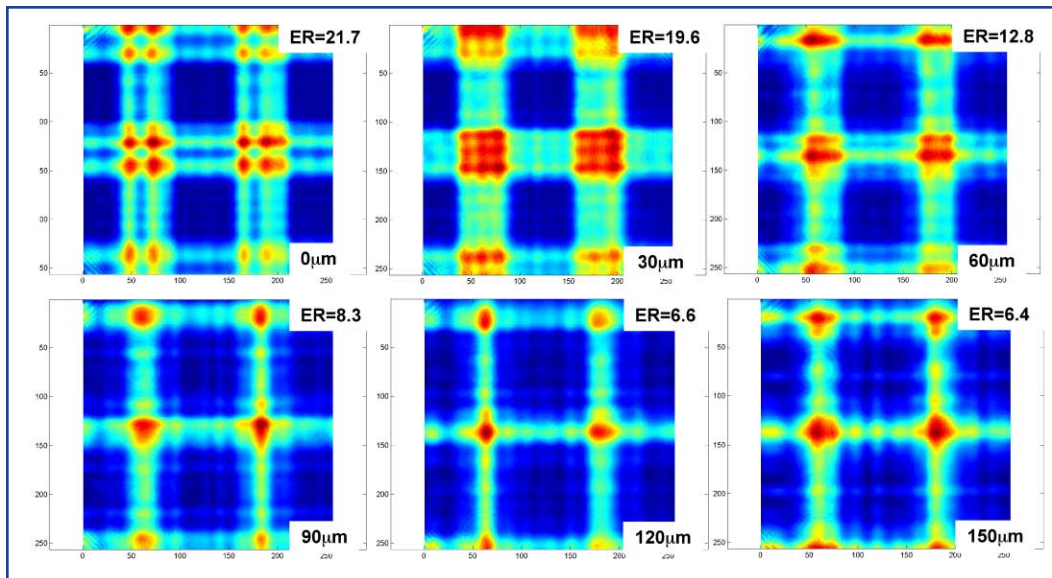


Figure 4: Measured irradiance patterns (red is highest) and corresponding extinction ratios (ER) through super pixel arrays as propagation distance is increased.

In principal, the extinction ratio of a polarizer will degrade as the component aperture decreases toward wavelength dimensions. However, Figure 3 illustrates that single pixelated micropolarizers fabricated at Sandia have measured extinction ratios still larger than 100:1 for pixel sizes as small as 9 microns. That exceeds, by seven times, previously reported extinction ratios for large area, 1 cm apertures. Equally important, the transmitted signal remains above 50%.

Overall, infrared polarimetric imaging can be accomplished with this new technique. However, due to near-field and diffractive effects of the finite component apertures, the distance between the micropolarizer array

and the FPA is critical to performance of the imager. This is shown in Figure 4, where there is a substantial change in the imaged pattern and a corresponding drop in extinction ratio (ER) with propagation distance and the subsequent introduction of adjacent super pixels (crosstalk). Because of these findings, it is now recommended that only a few microns separate components in the assembly process.

Computers and Information Sciences

Multiscale Computational Material Methods

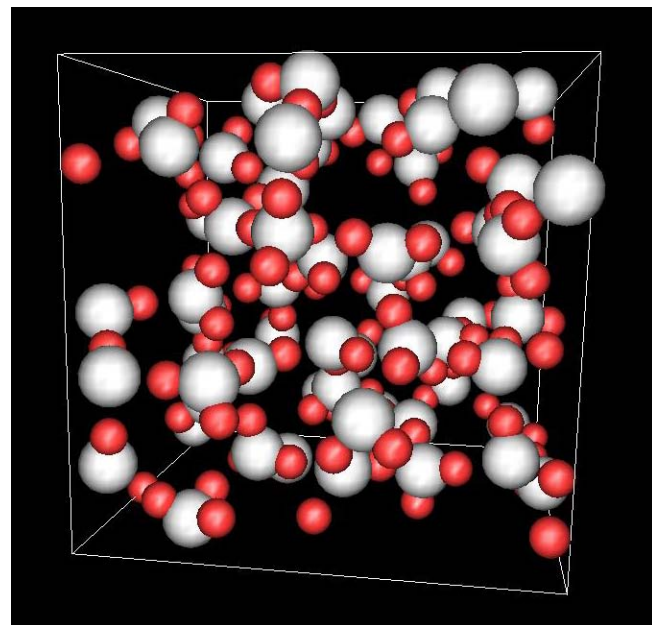
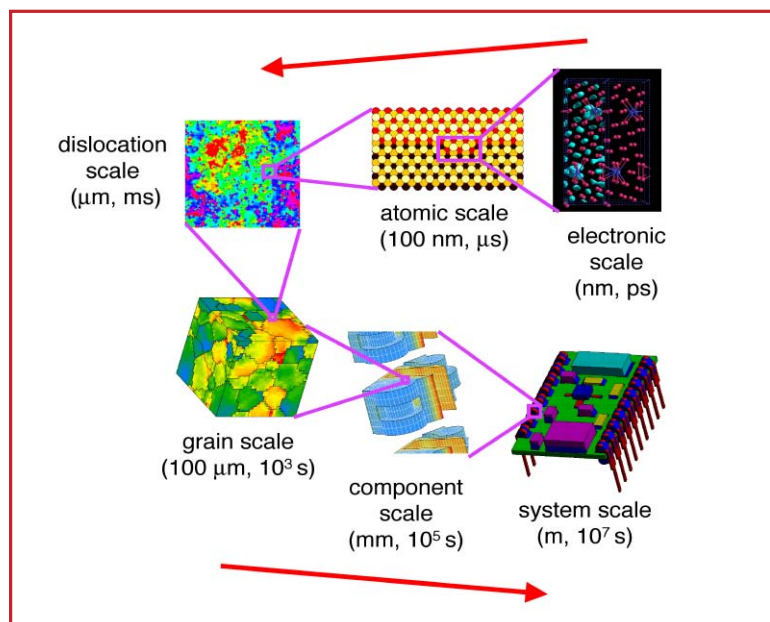


Figure 1: (left) DFT calculations on the electronic scale are the underpinning of many predictive multi-scale efforts at Sandia. (Image courtesy E. Holm).

Figure 2: (right) To obtain a correct description of water, not only are large supercells needed, but also molecular dynamics simulations over tens of pico seconds are needed in order to account for temperature effects. This requires an XC functional that is both fast and accurate. The picture shows a snapshot of a DFT-MD simulation using AM05 for 64 water molecules.

The AM05 density functional enables accurate and fast quantum simulations of condensed matter systems.

Enabling Predictive Multiscale Modeling and Simulations

Quantitative results for a broad range of systems in combination with a relatively low computational cost have made density functional theory (DFT) the foundation of most large-scale quantum mechanical simulations in science. Thus DFT is the workhorse method for high-fidelity quantum calculations at the electronic scale that are the basis for many predictive material simulations at larger scales (Figure 1). DFT simulations are helping solve some of the most difficult materials problems: describing radiation effects in semiconductor materials; materials behavior under extreme conditions, such as that encountered in high energy-density physics experiments at Sandia's Z-accelerator; or unveiling how ion selection occurs in biological systems.

At the core of each DFT electronic energy calculation lays the exchange-correlation

(XC) functional, which sets the limit for the accuracy of the calculations. Theory tells us that a "divine" XC functional exists with which DFT calculations provide the correct electronic ground state. Because this functional is not known, many approximate functionals must have been developed. The lack of systematic improvement in functionals for solid-state systems has made it difficult to predict which one is the most accurate for a given problem. The development of new functionals is thus critical to the progress of not only computational materials science, but also that of physics and chemistry in a broad sense. Since DFT is increasingly being employed for large systems (Figure 2) of several hundred atoms, and for long molecular dynamics simulations (tens of ps), the tradeoff between speed and

Technical Contact:
Ann Mattsson, Pd.D.
505-844-9218
aematts@sandia.gov

Science Matters Contact:
Alan Burns, Ph.D.
505-844-9642
aburns@sandia.gov

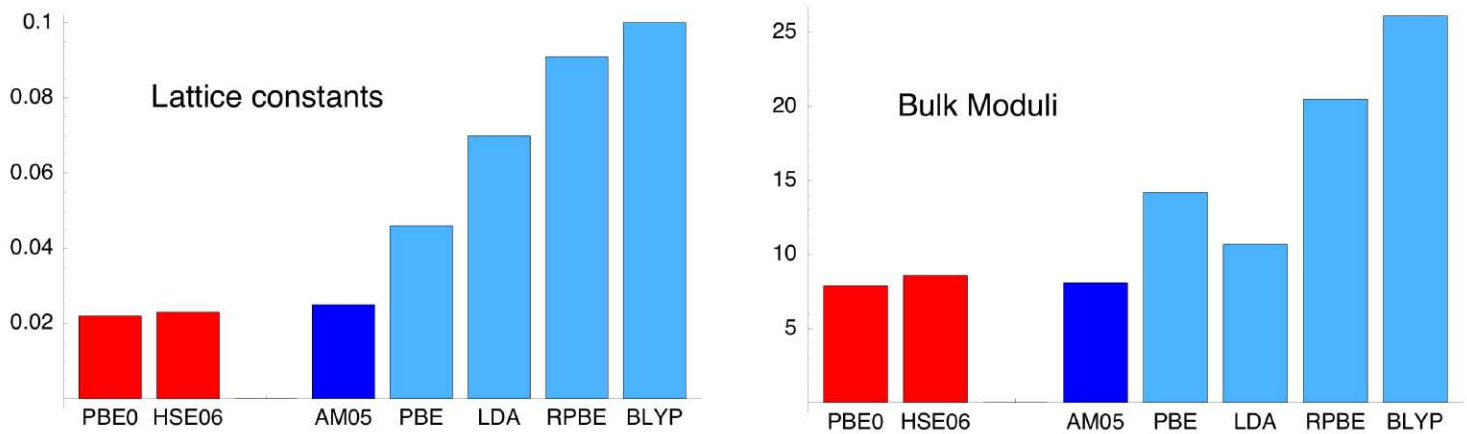


Figure 3: Comparison of mean absolute errors (MAE) for properties of 20 solids calculated with seven different functionals. The left panel shows lattice constants MAE in Ångström (0.1 nm) and the right panel shows bulk moduli MAE in GPa. Generalized gradient approximation type functionals (blue) are one to three orders of magnitudes faster to use than hybrids (red). AM05 has the same accuracy as hybrids for solids, and thus enable accurate and fast DFT calculations of defects in semi-conductors. It also allows for the use of DFT-MD as an accurate tool in Equation of State construction.

accuracy is arising as an additional major concern in functional development.

There is a fundamental difference between the behavior of electronic wave functions in a bulk solid and regions at surfaces and in interstitial regions in semiconductors. In the former, the wave functions are periodic propagating waves while in the latter, they are damped evanescent surface waves. By first identifying, and then focusing on this duality, we succeeded in developing a functional with high accuracy while retaining low complexity and thus high speed. For solids, the AM05 (Armiento and Mattsson, 2005) XC functional is proving to be as accurate as the best available XC functionals (Figure 3), while allowing one to three orders of magnitudes faster calculations. A calculation of a defect in a semiconductor like GaAs that runs overnight (12 hours) using AM05 would take almost six weeks using the fastest of the accurate functionals used up to now (HSE03/HSE06). Hence, AM05 is emerging as the functional of choice for accuracy as well as speed for essentially all materials.

Even so, there is more work to be done. Neither AM05 nor any other existing functional can treat dispersive forces or van der Waals binding, such as are prevalent in two important classes of materials, biomolecules and molecular solids, the latter of which includes high explosives and energetic materials. At Sandia, there is a focus on rational compound design, where it is of utmost importance to be able to obtain the right trends so that a target property can be calculated as a function of chemical composition. These applications require yet another leap in understanding and efficiency.

Publications:

“The AM05 density functional applied to solids”, Ann E. Mattsson, Rickard Armiento, Joachim Paier, Georg Kresse, John M. Wills, and Thomas R. Mattsson, *Journal of Chemical Physics*, to be published 07 February 2008.

“Functional designed to include surface effects in self-consistent density functional theory”, Rickard Armiento and Ann E. Mattsson, *Physical Review B* **72**, 085108 (2005).

“In Pursuit of the ‘Divine Functional’”, Ann E. Mattsson, *Science* **298**, 759 (25 October 2002).

“Designing meaningful density functional theory calculations in materials science—a primer”, Ann E. Mattsson, Peter A. Schultz, Michael P. Desjarlais, Thomas R. Mattsson, and Kevin Leung, *Modelling and Simulation in Materials Science and Engineering* **13**, R1-R31 (2005).



Microelectronics and Microsystems Advanced Microfabrication

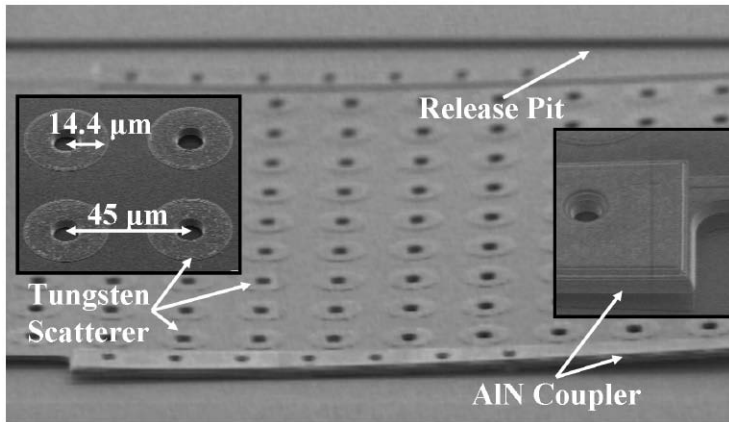


Figure 1: SEM image of a suspended 67 MHz acoustic crystal.

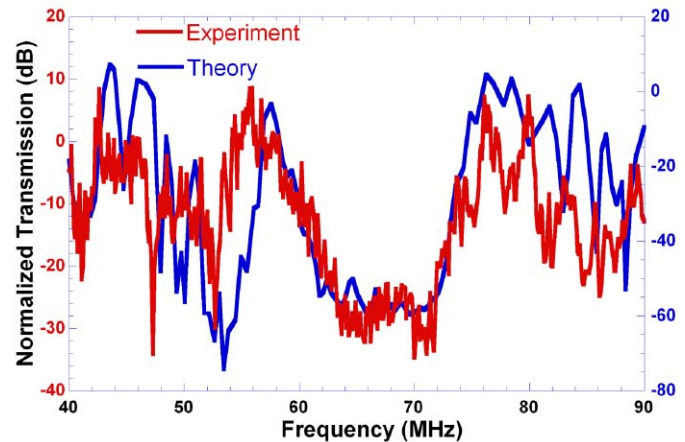


Figure 2: Measured and theoretical acoustic transmission.

Synthetic Acoustic Bandgap Materials

New microfabricated materials offer unique capabilities to control acoustic wave propagation and frequency distribution.

For more information:

Technical Contact:
Roy Olsson
505-284-6375
rholsson@sandia.gov

Science Matters Contact:
Alan Burns, Ph.D
505-844-9642
aburns@sandia.gov

An acoustic bandgap (ABG) is the acoustic wave equivalent of an electronic or photonic bandgap, where a wide range of frequencies are forbidden to exist in a structured material. ABGs thus offer the unique capability to control the propagation and distribution of acoustic waves or phonons. This, in turn, provides a new research tool for studying phonon interactions, and is applicable to acoustic devices such as radio frequency (RF) resonators and filters, ultrasound, and thermal management. The majority of applications and novel physics enabled by ABG materials require solid, low loss structures operating in the 10 MHz to 100 GHz regime with length scales ranging from 100 μm to 10 nm. Prior ABG work has been limited to large, hand-assembled structures operating at frequencies below 1 MHz. Now, Sandia researchers are utilizing advanced microfabrication and modeling capabilities to scale ABG devices to sub-micron length scales and to frequencies in excess of 1 GHz, where the full potential of this technology can be realized.

Shown in Figure 1 is a scanning electron microscope (SEM) image of a micromachined acoustic crystal. The micro-ABG is comprised of a lattice of high acoustic impedance tungsten scatterers in a low acoustic impedance silica medium. Inter-

rogation of the ABG is accomplished by aluminum nitride piezoelectric couplers, integrated on both sides of the bandgap material, that generate and detect acoustic waves. The measured and theoretical transmission of phonons through the ABG material versus frequency, normalized to the phonon transmission through a solid piece of silica, is shown in Figure 2. A wide bandgap is observed between 63 and 72 MHz, where acoustic transmission is attenuated by greater than 25 dB.

Micro-ABGs are very useful for acoustic isolation of microfabricated devices such as RF resonators and sensors. They can also be fabricated in ways to create novel devices in the acoustic crystal. For example, defects in the micro-ABG lattice through removal of W rods (Figure 3) have already been used to realize miniature acoustic waveguides that have applications in ultrasound and signal processing. In the future, defected acoustic crystals will be used to realize "mirrors" for micro-cavities, thus providing higher frequency selectivity than competing technologies. As the ABGs are scaled to even smaller sizes operating at higher frequencies, applications in thermal management and engineering the thermal noise distribution of a material become feasible.

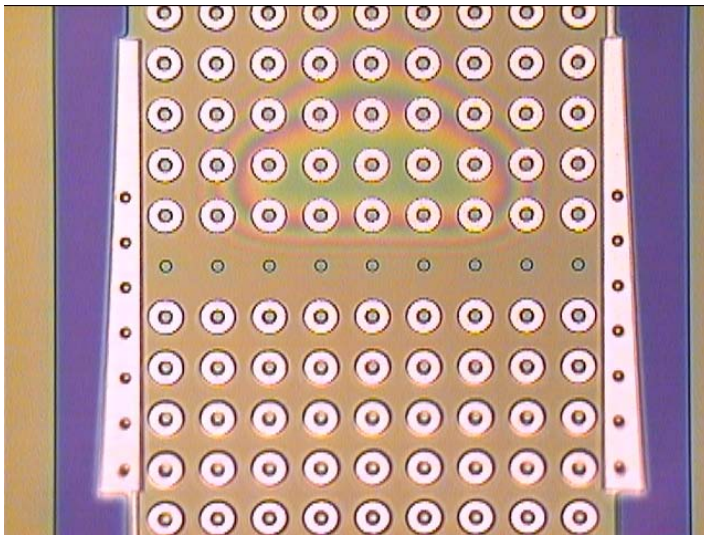


Figure 3: W1 acoustic waveguide realized by removing a single row of W rods from the acoustic crystal.

Publications

R. H. Olsson III, I. F. El-Kady, M. F. Su, M. R. Tuck, and J. G. Fleming, "Microfabricated VHF Acoustic Crystals and Waveguides," *Sensors and Actuators A: Physical*, In-Press.

R. H. Olsson III, J. G. Fleming, I. F. El-Kady, M. R. Tuck, and F. B. McCormick, "Micromachined Bulk Wave Acoustic Bandgap Devices," *International Conf. on Solid-State Sensors, Actuators, and Microsystems*, pp. 317-321, June 2007.

J. G. Fleming, R. H. Olsson III, I. El-Kady, and M. Tuck, "CMOS Compatible, Electrically Transduced, Acoustic Bandgap Structures," *International Symposium on Photonic and Electro-magnetic Crystal Structures*, April 2007.

I. El-Kady, J. G. Fleming, R. H. Olsson III, and T. S. Luk, "Modeling of Micromachined Acoustic Bandgap Structures and Devices," *International Symposium on Photonic and Electro-magnetic Crystal Structures*, April 2007.

Patent Applications

R. H. Olsson III, J. G. Fleming, I. F. El-Kady, and F. B. McCormick, "Microfabricated Bulk Wave Acoustic Bandgap Device," United States Patent Application, 11/748,832, May 2007.



Computers and Information Sciences Architectures

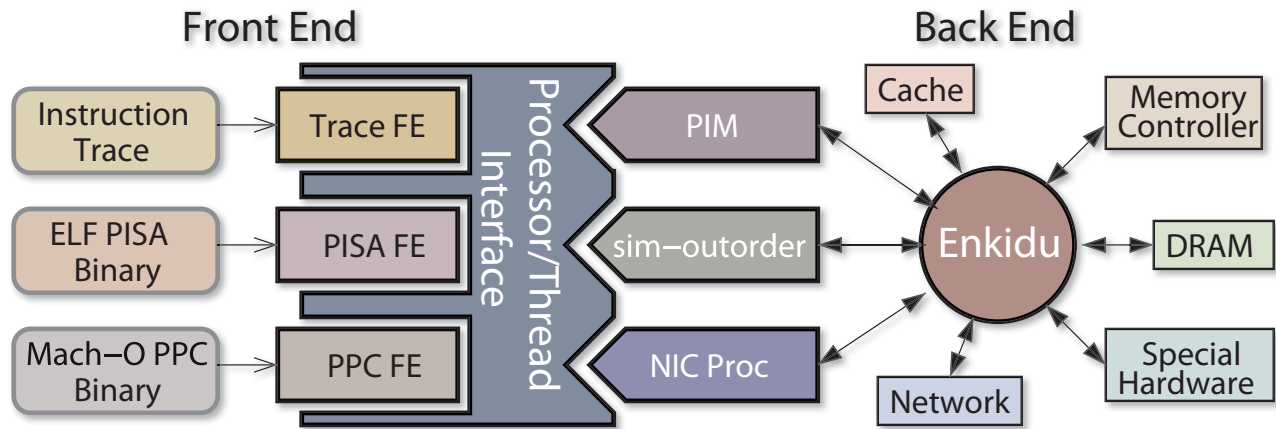


Figure 1: To encourage flexibility, the SST is comprised of “front end” modules which simulate software execution and “back end” modules which model hardware components.

The Structural Simulation Toolkit: Designing the Next Generation of Computers and Networks

Toolkit identified bottlenecks in Red Storm network and will help design more efficient networks for future supercomputers.

For more information:

Technical Contact:
Arun Rodrigues
505-284-6090
afrodri@sandia.gov

Science Matters Contact:
Alan Burns, Ph.D
505-844-9642
aburns@sandia.gov

High performance computer modeling and simulation is a foundational capability that underlies much of Sandia’s core missions. The growing technical complexity of this work requires computers of immense power and sophistication. It is becoming increasingly difficult, however, for traditional computer architectures to grow with these challenging demands, requiring us to find new ways of organizing processors, memory systems, and networks. To guide the design and construction of the next generation of supercomputers, Sandia has developed the Structural Simulation Toolkit (SST). The SST allows fast exploration of novel hardware structures and innovative software techniques.

The SST accurately simulates each cycle of a computer system. It is built from Enkidu, a simulation package that models interactions between the different hardware pieces of a system and coordinates their internal actions. It is capable of simulating a number of components, including advanced networks (such as the Red Storm SeaStar network), modern processors, and complex memory hierarchies. By using a modular structure (Figure 1), the SST allows users to quickly reconfigure their design,

adding new components and reorganizing existing ones. This flexibility has allowed the SST to explore a number of issues, such as network hardware to accelerate message processing (Figure 2), multithreaded processing, and processing-in-memory. In the case of the Red Storm’s SeaStar network, the simulation identified bottlenecks, and will help design more efficient networks for future supercomputers. The SST is currently being used by a number of sites across the country to explore issues in compilers, language development, advanced packaging, and transactional memory.

Achieving new levels of computer scalability and performance is critical to support Sandia’s science and engineering simulations. Several LDRD projects have used the SST to explore improved floating point architectures and processing-in-memory. With current architectures unable to provide the necessary performance, new hardware and software concepts must be explored and evaluated. The SST provides a simple, modular framework to quickly develop future architectures.

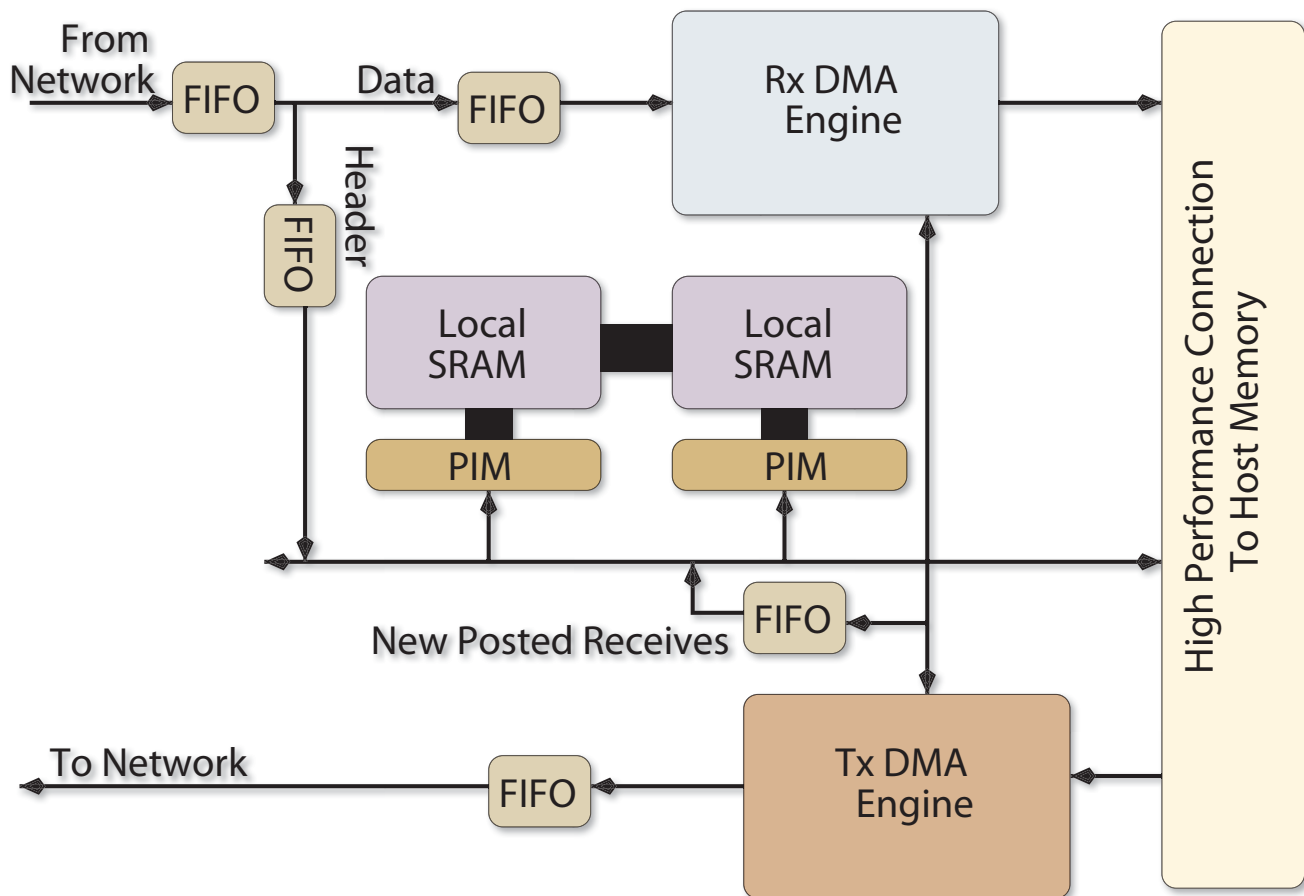


Figure 2: The simulator was used to simulate multi-threaded processors integrated into a network interface to improve message processing.

References:

Arun Rodrigues, Richard Murphy, Peter Kogge, Jay Brockman, Ron Brightwell, and Keith Underwood. "Implications of a PIM Architectural Model for MPI." In Proceedings the 2003 IEEE Conference on Cluster Computing, December 2004.

Keith D. Underwood, Michael Levenhagen, and Arun Rodrigues. "Simulating Red Storm: Challenges and Successes in Building a System Simulation," in 21st International Parallel and Distributed Processing Symposium (IPDPS'07), March 2007.

Arun Rodrigues, Patrick La Fratta, Richard Murphy, Kyle Rupnow, Keith Underwood, and Katherine Compton. "Micro-processor Extensions to Accelerate Scientific Applications," SAND2007-6206. September 2007.



Pulsed Power Science & Technology Enabling Capabilities



Figure 1: *Left* - Sandia researcher Matt Higgins conducts a propagation experiment at the Sago. *Right* - Sandian Dawna Charley (left) and a Sago mine worker prepare a vehicle before it enters the mine.

Measurement and Modeling of Electromagnetic Propagation of Lightning Energy into the Sago Mine

Sandia team verifies that lightning could have caused 2006 explosion.

For more information:

Technical Contact:

Larry Schneider
505-845-7135
lxschne@sandia.gov

Science Matters Contact:

Alan Burns, Ph.D
505-844-9642
aburns@sandia.gov

On January 2, 2006, a methane gas explosion killed 12 miners at the Sago underground coal mine in West Virginia. Lightning was quickly considered a possible cause of the accident. Eyewitness accounts describe strong thunderstorm activity above the mine at the time of the blast. More incriminating were the simultaneous recordings of cloud-to-ground lightning in the vicinity of the surface above the mine, a spike in carbon monoxide inside the mine (indicating an explosion), and seismic activity of the blast. While the circumstantial evidence was strong, a scientific explanation was missing of how lightning could propagate into the sealed area 300 feet underground and 2 miles from the mine entrance.

A Sandia team, working at the mine with the Mine Safety and Health Administration (MSHA), took measurements to characterize electromagnetic propagation through the earth and via metallic penetrations (coal conveyor, rails, and power and com-

munication lines) into the mine (Figures 1). Measurements were made in the frequency range typically seen in natural lightning strokes. Each metallic penetration into the mine was characterized over this frequency range at various points from the mine entrance to the sealed area, 2 miles away. While these penetrations did not breach the sealed area where the blast initiated, they were conduits for electrical energy into the mine.

For measuring propagation of lightning energy from the surface to the mine cavern 300 feet below, the drive signal was applied to a long wire stretched on the surface. Directly below, inside the sealed area, an antenna received the transmitted signals. Electric field and voltage measurements were mapped and compared favorably to analytical models simulating lightning propagation through the earth. They then were combined analytically with mathematical representations of natural lightning strokes to calculate induced voltage on an



abandoned pump cable in the sealed area. The conclusion was that lightning near the surface above the sealed area could have generated sufficiently high voltage on the pump cable to create a spark that initiated the methane explosion.

This pivotal work led MSHA to set in motion changes in mining operations to reduce the probability of such a catastrophic event occurring in the future. Mine safety can be improved with a better understanding of this phenomenon in the variety of scenarios seen in the U.S. mining system.



Microelectronics and Microsystems Photonics

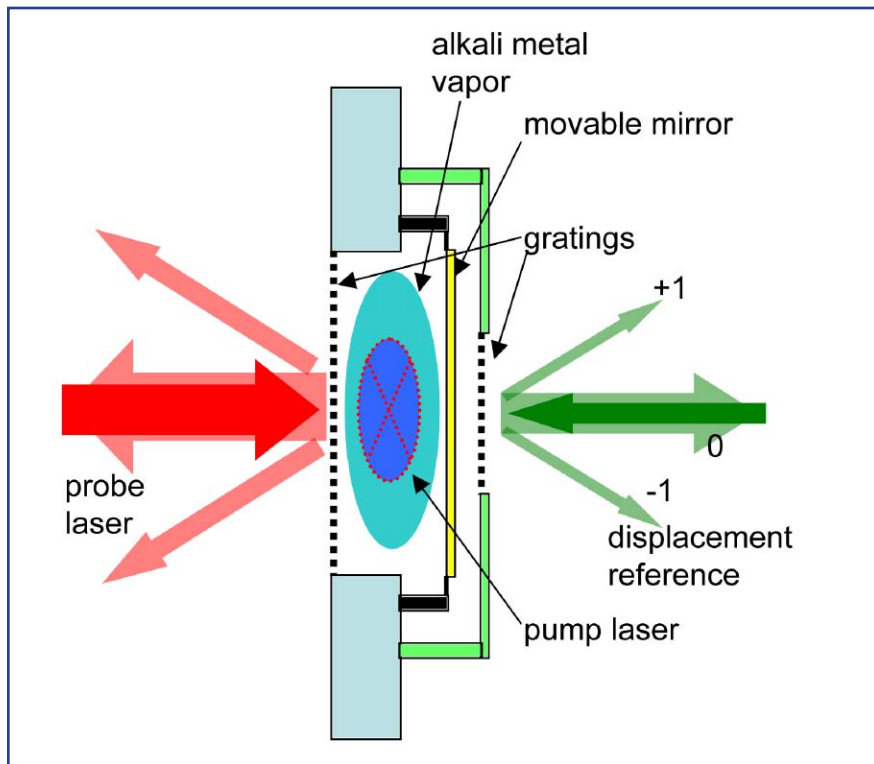


Figure 1: Schematic of the atomic magnetometer micro-cavity. A movable mirror and a grating are placed on either side of the atomic vapor cell. A pump laser (blue) orients the atomic spins. A probe laser (red) passes through the grating and the atomic vapor before reflecting off the mirror. The reflected light then passes through the grating again and interferes with light that is reflected directly from the grating. As the atoms respond to a magnetic field, their index of refraction changes, causing the interference pattern from the grating to shift. The displacement reference beam (green) precisely locates the movable mirror.

Atomic Magnetometers

Atomic magnetometers offer low power and high sensitivity in a small package.

For more information:

Technical Contact:

Peter Schwindt
505-845-4040
pschwin@sandia.gov

Science Matters Contact:

Alan Burns, Ph.D
505-844-9642
aburns@sandia.gov

High sensitivity detection of magnetic fields is a fundamental capability that enables a large number of diverse applications, from locating unexploded ordnance and underground structures, to the detection of biomagnetic fields associated with heart and brain activity. Superconducting magnetometers have long been the only practical option for high sensitivity magnetic field detection. However, they require bulky and expensive cryogenic cooling. Recent advances in atomic magnetometry have allowed world-record sensitivity (less than one femtotesla) to be achieved without the use of cryogenic cooling, thus drastically reducing the size and operating expense of a magnetometer. At Sandia, researchers are applying their photonics expertise to advance this new technology.

Atomic magnetometers rely on the fact that an alkali atom has an unpaired electron in its outer shell whose spin rapidly precesses in an external magnetic field. In Figure 1, a

resonant (pump) laser beam shines through an atomic vapor cell to orient the atomic spins, and a second (probe) laser beam passes through the vapor to detect how the spins react to the magnetic field. The highest possible sensitivity is achieved when the magnetometer is operated at a low magnetic field. In this regime, atom-atom collisions in the atomic vapor are no longer a source of decoherence, and thus the number of atoms participating in the magnetic field measurement can be dramatically increased.

One aspect of Sandia's effort in atomic magnetometry focuses on miniaturization. To maintain high sensitivity at small sizes, a tunable micro-cavity is being developed for improved optical detection of the atomic response to a magnetic field (Figure 1). The tuning element in the cavity is a moveable microelectromechanical (MEMS) mirror (Figure 2). To contain the atoms in a small volume that also allows good optical access for the

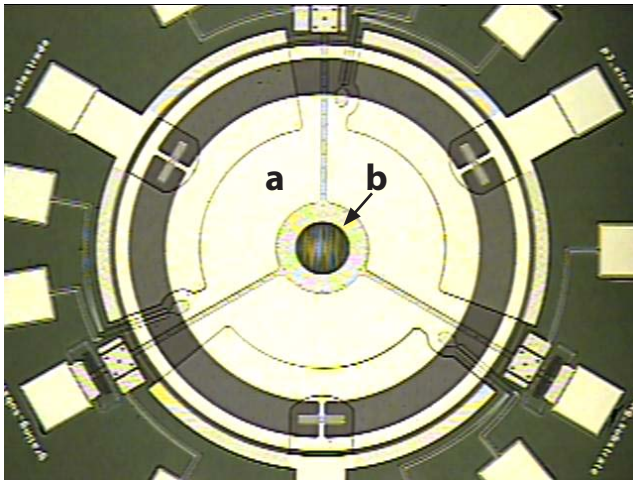


Figure 2: Photo of the movable MEMS silicon mirror and grating structure. (a) indicates the mirror (~1 mm diameter) and (b) indicates the grating.

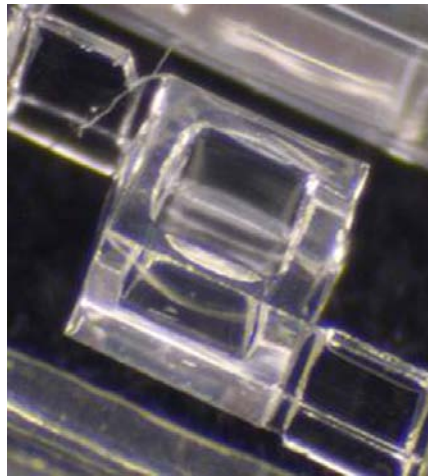


Figure 3: Photo of the patterned glass cell prior to filling with the alkali metal vapor.

lasers, a 1 mm³ vapor cell is being developed using a photo-patternable glass (Figure 3).

In another effort, an atomic magnetometer is being developed for magnetoencephalography (MEG), the detection of the extremely weak magnetic fields produced by the brain. MEG data is collected by surrounding the head with an array of magnetometers and is then used to infer the location of neural currents inside the brain. Being one of the few non-invasive techniques for measuring brain activity, both spatially and temporally, MEG is a critical tool for furthering our understanding of the physiology underlying human cognitive processes.

The design challenge is to attain high sensitivity while keeping in mind the requirements of the human subject. A major component of the effort will be to collaborate with

MEG experts at the Mental Illness and Neuroscience Discovery (MIND) Institute and the University of New Mexico to provide us guidance in the design and use of the device for use with animal models and human subjects. The high spatial resolution of MEG comes from using multiple sensors around the head. Because the atomic magnetometer reads out the atomic response to a magnetic field via optical interrogation, we can readily achieve multi-channel operation by simply detecting separated regions of the probe laser beam. Techniques developed in these research efforts will push the state of the art in atomic magnetometry, and, when combined, will enable many strategic applications, including underground structure mapping, remote sensing for boarder security, and MEG.



Computers and Information Sciences Cyber Security



Figure 1: Example of a “SHINI” heat map. The counts (and corresponding colors in the heat chart) represent the number of distinct connections from that country over approximately 60 seconds.

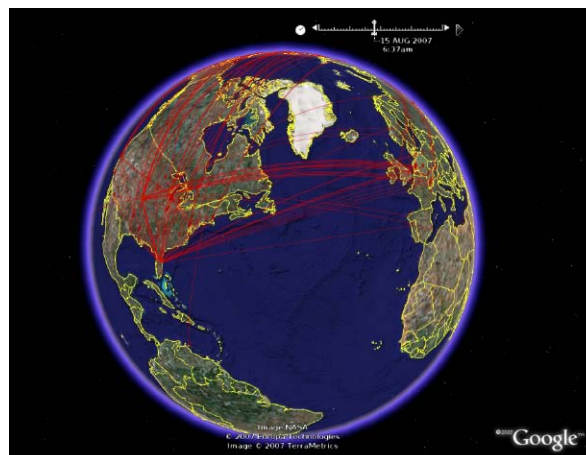


Figure 2: Example of a “SHINI” point map.

Geo-Temporal Visualization of Internet Activity

*Student-developed
programs help analysts
detect trends.*

Internet-connected computers are subject to attacks at all hours of the day and night from anywhere in the world. Intrusion detection analysts at Sandia, and their counterparts at other large organizations, need tools that allow them to visually display important information, such as when and where network connections originated, from their enormous security logs (typically measured in gigabytes of data). Such a tool would not only allow analysts to identify cyber attacks not readily apparent at first glance in the logs, but would also easily illustrate the origin of the attacks to a non-technical audience or customer. This is an example of geo-temporal visualization: displaying location and timing information together.

Intrusion detection analysts at Sandia tasked participants from Sandia’s Center for Cyber Defenders student intern program to develop a computer program that uses geo-temporal visualization for security log data. Two students came up with an idea that works in conjunction with the popular application “Google Earth” that displays the activity in a variety of forms. This program is called “SHINI” (Sandia Heuristic Intelligent Network Imaging).

One way SHINI can visualize geo-temporal information is called a “heat map,” similar

to a weather map, where the color of a country is determined by the current number of connections from that country (Figure 1). The heat map can either display real-time log information or display a time-lapse visualization. Using time-lapse visualization, an analyst can view information from a period of days in a matter of minutes.

Another available visualization is a “point map.” As shown in Figure 2, each network connection would be represented by a point on the map. When used in conjunction with the capability to link plotted points together, the results look similar to an airline route map. This capability can be extremely useful when logs from different sources are combined. As with heat maps, point maps can display both real-time and time-lapse information.

While the current SHINI program is constructed to accept network logs as input, these programs can be easily modified to accommodate virtually any data files that include time and location information. Thus, SHINI could be used in any number of situations where simple-to-use, real-time and time-lapse geo-temporal visualization can help analysts and investigators.

For more information:

Technical Contact:
Steven Hurd
925-294-1224
sahurd@sandia.gov

Science Matters Contact:
Alan Burns, Ph.D
505-844-9642
aburns@sandia.gov





Computers and Information Sciences Informatics

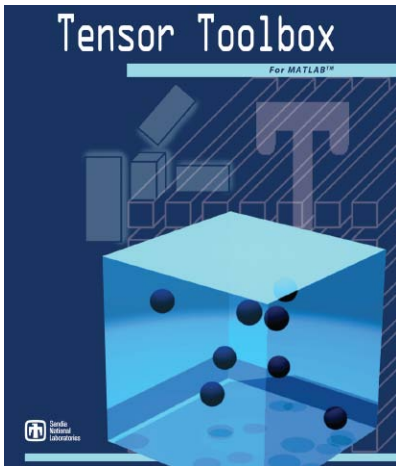


Figure 1: Tensor Toolbox software package

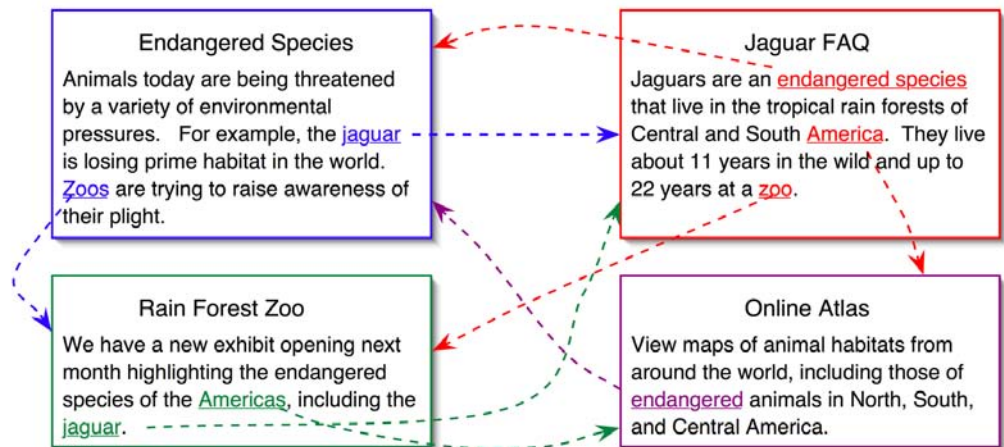


Figure 2: Four web pages with connecting links

Tensor Toolbox for MATLAB™

Sandia's Toolbox allows scientists to solve large, sparse tensor calculations on very large data sets.

Life is multi-dimensional, so it might be surprising to realize that nearly all calculations and simulations are done using two-dimensional mathematical arrays, better known as matrices. Even large-scale, three-dimensional engineering simulations, four-dimensional physics calculations, and multi-dimensional data analysis methods have been structured and optimized to work as two-dimensional matrix calculations. These computational approximations result in slower or less accurate calculations.

Sandia scientists and colleagues are at the forefront of new research in algorithms and software for applying multi-dimensional arrays, called tensors, to solve multi-dimensional problems that arise in data analysis, signals processing, image recognition and analysis, and other fields.

A major roadblock to the use of these multi-dimensional techniques was the absence of any software for large, sparse tensor calculations. Sparse tensors have a majority of entries that are zero. Only the non-zero entries are usually stored. Sandia scientists developed the Tensor Toolbox for MATLAB™ (Figure 1) to address this need. The free software integrates with MATLAB™, the matrix-based high-level language and

interactive environment that enables users to perform computationally intensive tasks faster than with traditional programming languages. The Tensor Toolbox makes working with tensors in MATLAB™ as easy as working with matrices. The user need not worry about the low-level details to do complex, high-level operations, and the tool can handle very large problems such as sparse tensors the size of 10,000x10,000x10,000 with a half-million nonzero entries.

Sandia's Tensor Toolbox has enabled new and more accurate analyses in multiple application domains, particularly those involving large amounts of data ("data mining"). For example, several web pages can have connecting links (Figure 2). The links in those web pages can be analyzed in a graph form with labeled edges (Figure 3), and thence stored as a sparse tensor (Figure 4). This higher-order web link analysis allows for better automatic grouping and labeling of web pages through the TOPHITS algorithm (also developed at Sandia).

Another application is in bibliometric analysis using multiple linkages (authors, documents, terms), including understanding author-keyword trends. An example is

For more information:

Technical Contact:
Tamara G. Kolda, Ph.D.
925-294-4769
tgkolda@sandia.gov

Science Matters Contact:
Alan Burns, Ph.D.
505-844-9642
aburns@sandia.gov

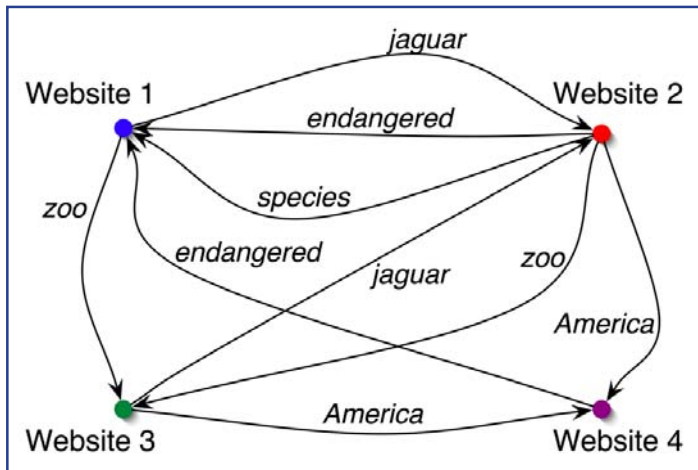


Figure 3: The linked web pages in Figure 2 are converted to a graph with labeled edges (stored as a tensor) and the link text is used in the analysis.

shown in Figure 5, where connections between cited authors and their publications are plotted in graph form. Similarly, national security applications of the Tensor Toolbox include temporal analysis of email exchanges, including automated discovery of conversation topics and sender/recipient roles over time.

Outside of Sandia, over one thousand registered users of the Tensor Toolbox have reported diverse applications including chatroom data analysis, continuum mechanics, online monitoring of network data, acoustic signal research, chemometrics, finite element computations, studies of bird migration, statistical computations, biochemical analysis, image classification, air traffic control studies, astronomy, models of tumor growth, character animation, computer vision, brain imaging, multidimensional economics, general relativity research, modeling optical systems, physics, multilayer absorption for photovoltaics, signal processing, computational differential geometry, neuro-fuzzy networks, and video analysis.

Tensor Toolbox Web Site

<http://csmr.ca.sandia.gov/~tgkolda/TensorToolbox/>

References:

Brett W. Bader, Richard A. Harshman, and Tamara G. Kolda. **Temporal analysis of semantic graphs using ASALSAN**. In *ICDM 2007: Proceedings of the 7th IEEE International Conference on Data Mining*, pages 33–42, October 2007.

Brett W. Bader and Tamara G. Kolda. **Efficient MATLAB computations with sparse and factored tensors**. *SIAM Journal on Scientific Computing*, July 2007.

Brett W. Bader and Tamara G. Kolda. **Algorithm 862: MATLAB tensor classes for fast algorithm prototyping**. *ACM Transactions on Mathematical Software*, 32(4):635–653, December 2006.

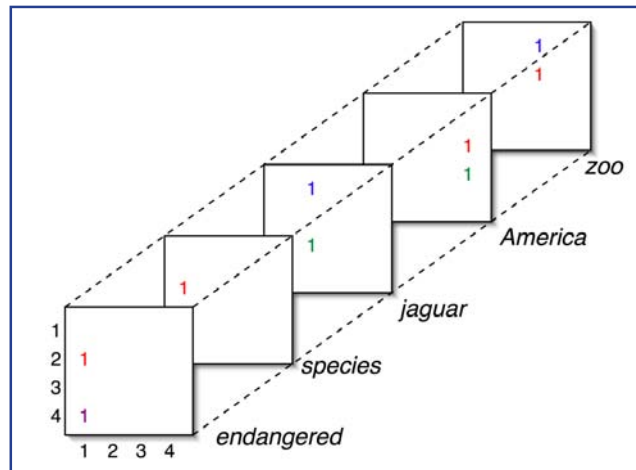


Figure 4: The resulting tensor representation of Figure 3 is extremely sparse. This tensor is decomposed using the Tensor Toolbox.

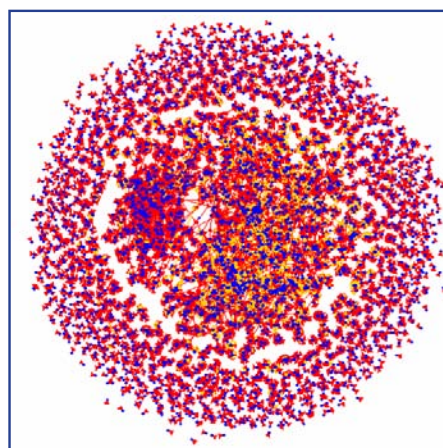


Figure 5: A graphical representation of 5000 papers (in blue), their authors (in red), and the citation and authorship connections between them.

Peter A. Chew, Brett W. Bader, Tamara G. Kolda, and Ahmed Abdelali. **Cross-language information retrieval using PARAFAC2**. In *KDD '07: Proceedings of the 13th ACM SIGKDD International Conference on Knowledge Discovery and Data Mining*, pages 143–152. ACM Press, 2007.

Daniel M. Dunlavy, Tamara G. Kolda, and W. Philip Kegelmeyer. **Multilinear algebra for analyzing data with multiple linkages**. Technical Report SAND2006-2079, Sandia National Laboratories, April 2006.

Tamara G. Kolda and Brett W. Bader. **Tensor decompositions and applications**. Technical Report SAND2007-6702, Sandia National Laboratories, November 2007.

Tamara Kolda and Brett Bader. **The TOPHITS model for higher-order web link analysis**. In *Workshop on Link Analysis, Counterterrorism and Security*, 2006.

Tamara G. Kolda, Brett W. Bader, and Joseph P. Kenny. **Higher-order web link analysis using multilinear algebra**. In *ICDM 2005: Proceedings of the 5th IEEE International Conference on Data Mining*, pages 242–249, November 2005.



Materials Science and Technology

Ultra-thin Films

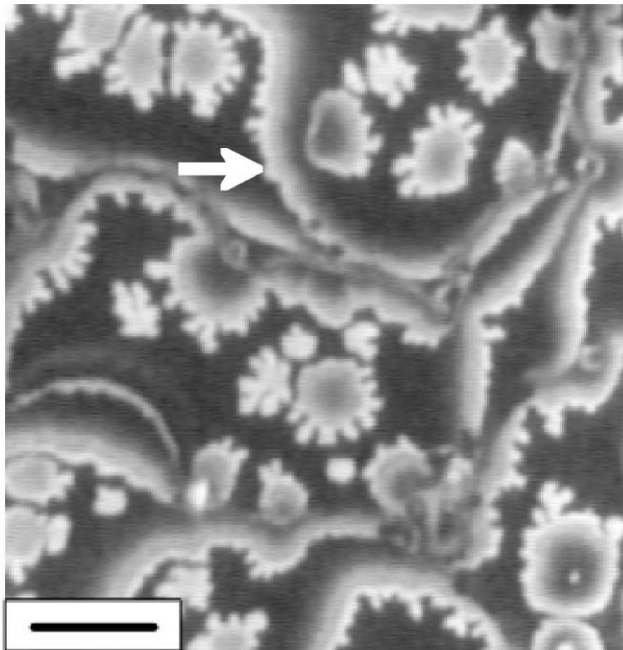
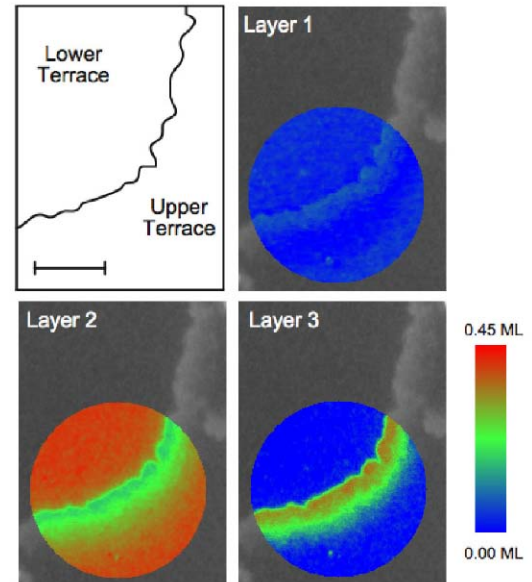


Figure 1: (Left) Low energy electron microscope (LEEM) image of a Cu(001) surface recorded after the deposition of ~ 0.6 ML Pd at 200°C . The white arrow points to a surface step. The continuous variation in intensity away from the step and its dendritic shape indicates highly non-uniform growth. (Electron energy = 13.1 eV; Scale bar = $1\ \mu\text{m}$).

Figure 2: (Right) Three-dimensional, color-coded map of the Pd concentration near a surface step. The images were constructed from the current-voltage (IV) analysis of 17,665 individual pixels. The maps are superimposed on the corresponding LEEM image at 13.1 eV. There is essentially no Pd in the top layer, maximum concentration in the second layer away from the steps, and a high concentration in the third layer near the steps. (Scale bar = 500 nm.)



Identifying the Origins of Heterogeneity in Ultra-thin Films

New technique provides three-dimensional maps of surface chemical composition.

For more information:

Technical Contact:
Gary Kellogg, Ph.D.
505-844-2079
gkello@sandia.gov

Science Matters Contact:
Alan Burns, Ph.D.
505-844-9642
aburns@sandia.gov

Thin films play a key role in many technologies. Applications range from promoting chemical reactions at surfaces for improved sensor, catalytic, or anti-corrosion properties to more exotic ones in nanotechnology, where reduced dimensionality gives rise to unique electronic or magnetic properties. It is well known that the mechanical, electrical, and catalytic properties of thin films are intimately related to structure and composition. However, understanding this relationship in detail is challenging because thin films are often inhomogeneous, especially at the nanoscale. Historically, measuring structural and compositional heterogeneity at these small length scales has proven difficult because high spatial resolution must be combined with sub-surface chemical sensitivity.

In collaboration with scientists at IBM, Yorktown Heights, and the University of New Hampshire, Sandia researchers have developed a technique to determine the three-dimensional (3-D) composition

profile of a surface with 10-nm lateral resolution and single atomic-layer depth sensitivity. The technique combines the high-spatial resolution of the low-energy electron microscope (LEEM) with the chemical sensitivity of quantitative electron reflectivity measurements. Using this technique, we have investigated how heterogeneity develops during the growth of ultra-thin Pd films on Cu(001). Such films have been identified as potential inhibitors to the undesired effect of Cu electromigration in microelectronic devices, but little is known about the initial stages of film growth. Figure 1 shows a LEEM image of a Cu(001) surface recorded during Pd deposition at 200°C . The spatial variation of the intensity shows directly that the surface is heterogeneous, but to determine how and why the inhomogeneity occurs requires detailed information on the distribution of Pd in the atomic layers just below the surface. From our analysis, we obtain color-coded maps (Figure 2) showing how the Pd concentration varies in the vicinity of a surface step. From the time-evolution of such 3-D compositional profiles, we discovered that

the heterogeneity observed in Figure 1 can be explained with a conceptually simple “step-overgrowth” model (Figure 3) in which step flow, caused by movement of the Cu atoms, converts mobile Pd in the second layer into fixed Pd in the third layer.

These results highlight the important role of surface steps in surface alloy formation and demonstrate how our new technique can give powerful insight into complex morphological evolution at surfaces.

Publications:

J. B. Hannon, J. Sun, K. Pohl, and G. L. Kellogg, “Origins of Nanoscale Heterogeneity in Ultra-thin Films,” *Phys. Rev. Lett.* 96, 246103 (2006).

J. Sun, J. B. Hannon, G. L. Kellogg, and K. Pohl, “Local Structural and Compositional Determination via Electron Scattering: Heterogeneous Cu(001)-Pd Surface Alloy,” *Phys. Rev. B* 76, 205414 (2007).

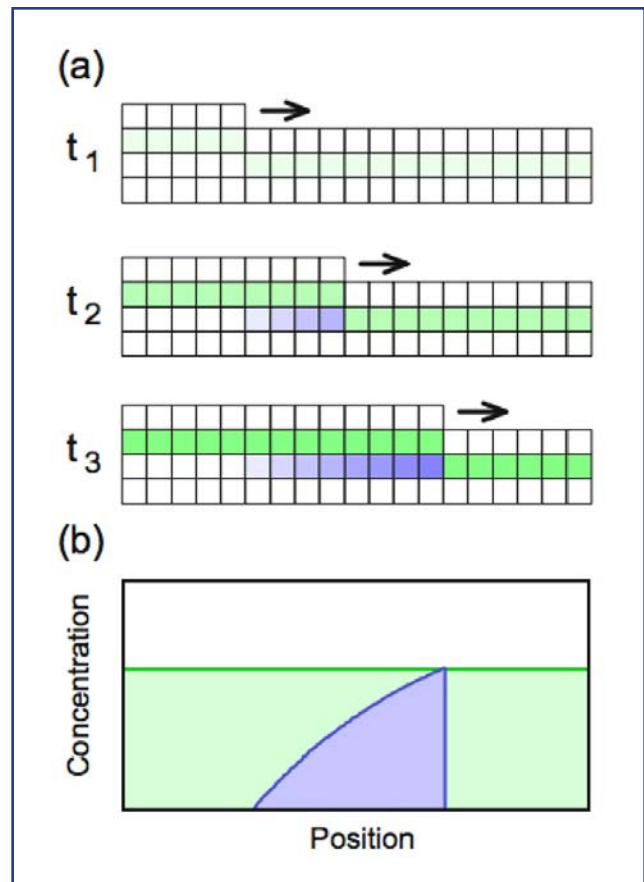


Figure 3: Schematic drawing illustrating how heterogeneity arises during step-flow overgrowth for Pd on Cu(001). (a) Side views of the Cu surface. The Pd composition in the second layer is shown in green, in the third layer blue. Step flow overgrowth converts mobile Pd in the second layer into fixed Pd in the third layer. (b) Spatial dependence of the Pd concentration in the second (green) and third (blue) layers at the end of growth.



Computers and Information Sciences Water Security

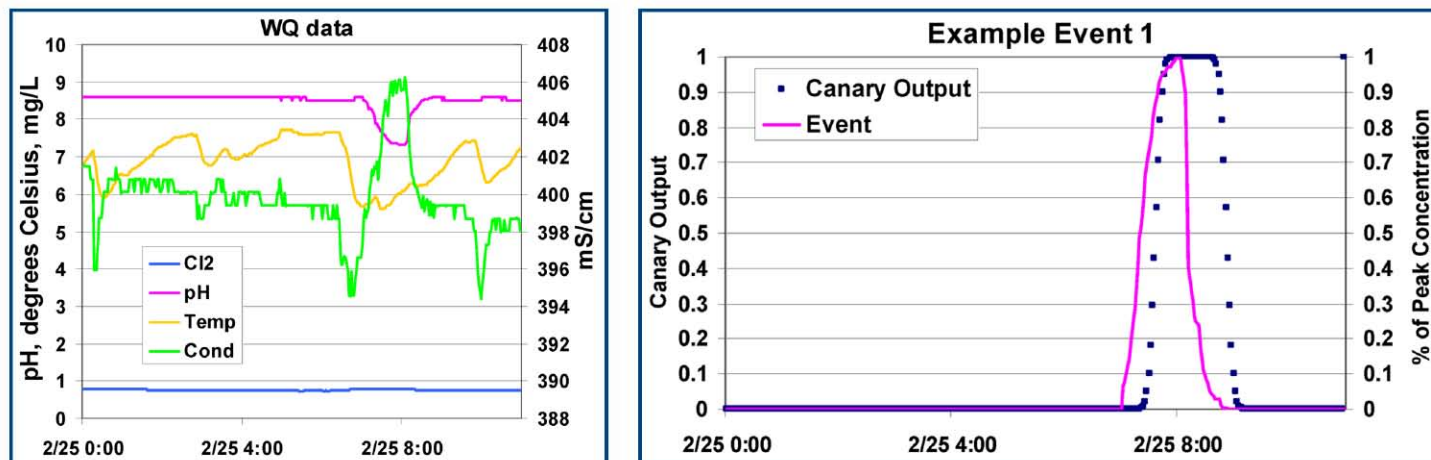


Figure 1: Canary software uses water sensor data (left) to detect contamination incidents (right), using water quality (WQ) parameters like chlorine levels (Cl_2), pH, temperature and turbidity (Cond).

Sandia Collaborates with the EPA to Develop Contaminant Warning Systems

Software deployed at several major water utilities

Technical Contact:
William Hart
505-844-2217
wehart@sandia.gov

Science Matters Contact:
Alan Burns, Ph.D.
505-844-9642
aburns@sandia.gov

A reliable, clean water supply is critical for maintenance of public health, protection of public infrastructure, and the normal operation of many industries. However, the distributed physical layout of drinking water systems makes them inherently vulnerable to contamination with deadly agents, resulting in potentially catastrophic numbers of illnesses or casualties. Sandia is currently partnering with the Threat Assessment Vulnerability Program (TEVA), within the Environmental Protection Agency's (EPA's) National Homeland Security Research Center, to develop contaminant warning systems (CWSs) for the protection of water supplies. A CWS uses sensors to monitor water quality and provide early detection of chemical or biological contaminants.

Sandia researchers have developed mathematical algorithms and software to address several CWS design challenges. Sandia's Canary software detects a change in water quality that indicates

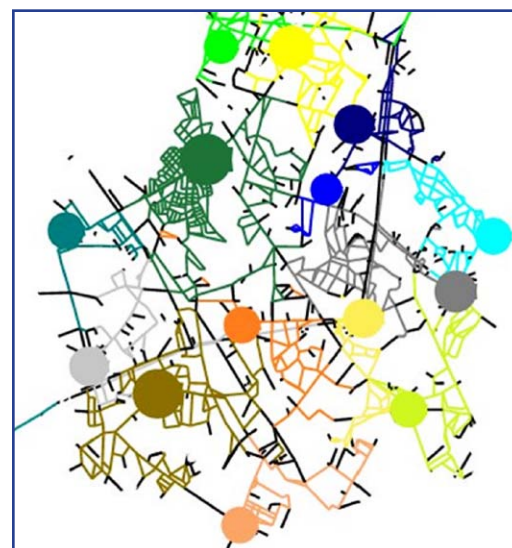


Figure 2: An example of how the TEVA-SPOT Toolkit optimizes sensors placements to simultaneously protect different subsets of a water distribution network.

a contamination incident, using data from commercially-available sensors that measure water quality parameters like pH and turbidity (Figure 1). A key issue is that many contaminant-specific sensors are not commercially available. Another key issue is the placement of sensors in large water distribution networks. To solve the latter problem, Sandia's TEVA-SPOT Toolkit optimizes sensor locations to protect the largest possible population from a broad set of contamination incidents (Figure 2). New algorithms were developed for

Canary and the TEVA-SPOT Toolkit to enable water utilities to analyze large-scale, noisy data sets. In particular, these algorithms are designed to work on commonly available computing resources so that authorities can determine sensor placement for a large network on a standard workstation.

The EPA's Water Security Initiative used these tools in a pilot study at the Greater Cincinnati Water Works. Canary has been deployed at 17 locations in their distribution network, where it is performing real-time detection. The EPA has also partnered with the American Water Works Association to design CWSs for seven other U.S. water utilities with large distribution networks. The sensor placements developed during these studies could significantly reduce potential health impacts. Moreover, an economic assessment predicts that these CWS designs could reduce economic impacts by billions of dollars.

Related Publications:

"Detecting Changes in Water Quality Data." S A McKenna, M P Wilson and K A Klise. *J. of the American Water Works Association*. (to appear)

"Impact of sensor detection limits on protecting water distribution systems from contamination events." S A McKenna, D B Hart and L Yarrington, *J. of Water Resources Planning and Management*. 132 (4), 2006. pp. 305-309.

"Sensor placement in municipal water networks with temporal integer programming models." J Berry, W E Hart, C E Phillips, J G Uber and J Watson. *J. Water Resources Planning and Management*. 132 (4). 2006. pp. 218-224.

"Robust optimization of contaminant sensor placement for community water systems." R Carr, H J Greenberg, W E Hart, G Konjevod, E Lauer, H Lin, T Morrison and C A Phillips. *Mathematical Programming Series B*. vol. 107. 2006. pp. 337-356.

"Sensor Placement in Municipal Water Networks." J Berry, L Fleischer, W E Hart, C A Phillips and J Watson. *J. Water Planning and Resources Management*. 131 (3). May 2005. pp. 237-243.